Impact of Channel Slope, Variable magnetic Field and Effective Prandtl Number on MHD Maxwell Fluid in the Presence of Heat Generation and Thermophoresis

George Buzuzi

Abstract—**The study examines the impact of inclined stretching sheet, aligned magnetic field and effective Prandtl number on MHD Maxwell fluid in the presence of thermophoresis and heat generation. By employing similarity transformations the given partial differential equations are converted into nonlinear ordinary differential equations which are then solved numerically using MATLAB bvp4c technique. The investigations reveal that enlargement of the effective Prandtl number enhances the temperature and concentration of the fluid and suppresses the magnitude of the fluid velocity. It is observed that the fluid concentration is highest when both the channel slope and magnetic field inclination angles assume least values provided the effective Prandtl number is greater or equal to unity or when both inclination angles attain maximum values when the effective Prandtl number is less than unity. Additionally, the fluid temperature profile is greatest when channel slope is maximal and magnetic field angle is minimal. It is also observed that enlarged inclination angles enhances the temperature profile for larger E_{pr} values and suppresses the temperature profile for smaller E_{pr} values. Finally, it is deduced that raising the value of the thermophoretic parameter reduces the skin friction and mass transfer rate, whereas the heat transfer rate is improved.**

Index Terms – **Maxwell fluid, effective Prandtl number, inclined channel, thermophoresis.**

I. INTRODUCTION

MANY industrial processes deal with Newtonian and non-Newtonian fluids. In this study we consider a non-Newtonian model and in particular Maxwell fluid. Maxwell fluids are non-viscous rate-type fluids which predict the fluid elasticity, viscosity and stress relaxation impacts.

Wenchaang *et al.* [30] examined unsteady viscoelastic Maxwell fluid flow between two parallel plates and Qi and Xu [18] applied Fourier and Laplace transform to find exact solution of an unsteady viscoelastic fluid with fractional derivative Maxwell model. Later, Noor [17] conducted a study to explore MHD Maxwell fluid flow over a stretching surface in the presence of chemical reaction and Soret effect. The influence of convection heat transfer and viscous dissipation on fractional MHD Maxwell fluid flow was considered by Boi *et al.* [2]. Farooq *et al.* [8] explored MHD Maxwell fluid containing nanoparticles caused by an exponentially stretching sheet. During the same period, Wang *et al.* [29] analyzed oscillatory Maxwell fluid flow passing through a rectangular tube. An investigation on oscillatory fluid passing through a tube of triangular cross section was carried out by Sun *et al.* [26]. Nadeem êt al. [16] disclosed the numerical analysis of MHD Maxwell fluid flow containing nanoparticles flowing past a stretching sheet. Most recently, Fetecau *et al.* [9] addressed the effect of a constantly oscillating wall on Maxwell fluid flow past a porous channel. During the same period, Loganathan *et al.* [11] investigated the impact of thermal radiation and Catteneo-Christov dual diffusion on MHD Maxwell fluid past a heated stretching sheet. Detailed analysis on Maxwell fluid flow has been carried out by numerous researchers, who among them are Haritha *et al.* [10], Loganathan *et al.* [12], Loganathan êt al. [13], Saleem *et al.* [21], Sandeep and Solochana [23].

The current investigation also examines the influence of thermal radiation on the Maxwell fluid. The impact of thermal radiation on fluid flow has been reported by several authors. Mgyari [14], Mgyari and Pantokratoras [15] and Buzuzi and Makanda [4] revealed that in optically thick medium the impact of the radiation parameter and the Prandtl number on the fluid cannot be studied independently but instead the combined effect of the two parameters called the effective Prandtl number is considered.

The surfaces upon which fluid flows vary in their geometry and the magnetic field applied may be normal or oblique depending on the flow geometry configuration. Raju *et al.* [19], Buzuzi [5], Sandeep and Sugunamma [22], Buzuzi and Makanda [4] and Dadheech *et al.* [7] carried out studies on aligned magnetic fields. Their studies showed that by raising the inclination angle of the magnetic field, the heat transfer rate is enhanced and the fluid velocity is diminished.

Exploration on fluid flow past oblique surfaces have re-

Manuscript received March 23, 2023; revised August 19, 2023;
George Buzuzi is a mathematics lecturer at Department of Mathematics and Physics, Cape Peninsula University of Technology, P O Box 1906, Belville, 7535, South Africa (phone: +27 82 971 3160; email: buzuzig@cput.ac.za).

ceived the attention of numerous researchers. Among them are Alam *et al.* [1], Uddin [27], Buzuzi *et al.* [3], Buzuzi [5], Buzuzi and Makanda [4] and Ramzan *et al.* [20].

Whereas most of the investigations done so far dealt with either aligned magnetic field or flow surface slope and not both, a few researchers have developed detailed analysis on the simultaneous impact of both aligned magnetic field and slope of fluid channel. Sivaraj and Sheremet [25], Buzuzi [5] and Buzuzi, Makanda [4] and Buzuzi [6] are among the few researchers who have investigated the effect of both aligned magnetic field and flow surface slope. Most of these researchers considered the impact of the inclination angles independently. However, Buzuzi [5], Buzuzi and Makanda [4] and Buzuzi [6] considered the simultaneous effect of both aligned magnetic field and flow surface inclination on MHD Newtonian flow. The current investigations seek to address the simultaneous role of both inclination angles on Maxwell fluid flow.

To the best of the author's knowledge, there is no work covered on aligned magnetic field, effective Prandtl number, channel slope, thermophoresis and heat generation on Maxwell fluid, hence impetus for the current investigation.

II. MATHEMATICAL DESCRIPTION

We consider a steady MHD flow of Maxwell fluid past an inclined stretching sheet in a porous medium with aligned magnetic field, thermophoresis and heat generation. We let the $x-$axis be directed along the inclined sheet and $y-$ axis directed perpendicular to it. The stretching sheet is inclined at an angle γ from the vertical. A uniform aligned magnetic field of uniform strength B_0 is applied at an angle α_1 to the flow direction. We assume that the magnetic Reynolds number is sufficiently small as to render the induced magnetic field negligible.

Under these assumptions and Boussinesq approximation, the governing equations for the boundary layer equations of continuity, momentum, energy and concentration can be stated as ([10], [17]):

$$\frac{\partial u_1}{\partial x}+\frac{\partial v_1}{\partial y}, \tag{1}$$

$$\begin{aligned} u_1\frac{\partial u_1}{\partial x}+v_1\frac{\partial u_1}{\partial y}+\lambda_t\left[u_1^2\frac{\partial^2 u_1}{\partial x^2}+v_1^2\frac{\partial^2 u_1}{\partial y^2}\right] \\ +2\lambda_t u_1 v_1\frac{\partial^2 u_1}{\partial x\partial y}=\nu\frac{\partial^2 u_1}{\partial y^2}-\frac{\nu}{K^*}u_1 \\ -\frac{\sigma {B_o}^2\sin^2\alpha_1}{\rho}\left[u_1+\lambda_t v_1\frac{\partial u_1}{\partial y}\right] \\ +g\left[\beta_T(T_1-T_{1\infty})\cos\gamma+\beta_M(C_1-C_{1\infty})\cos\gamma\right], \end{aligned} \tag{2}$$

$$\begin{aligned} u_1\frac{\partial T_1}{\partial x}+v_1\frac{\partial T_1}{\partial y}=\frac{\lambda_c}{\rho c_p}\frac{\partial^2 T_1}{\partial y^2}-\frac{1}{\rho c_p}\frac{\partial q_n}{\partial y} \\ +\frac{Q_1(T_1-T_{1\infty})}{\rho C_p}+\frac{\mu}{\rho c_p}\left(\frac{\partial u}{\partial y}\right)^2+\frac{\sigma B_0^2 u_1^2\sin^2\alpha_1}{\rho c_p}, \end{aligned} \tag{3}$$

$$\begin{aligned} u_1\frac{\partial C_1}{\partial x}+v_1\frac{\partial C_1}{\partial y}=D_b\frac{\partial^2 C_1}{\partial y^2}-\frac{\partial}{\partial y}\left(V_1^t.(C_1-C_{1\infty})\right) \\ -k_l C_1, \end{aligned} \tag{4}$$

The corresponding boundary conditions are

$$\begin{aligned} u_1=u_{1w}=a_1x,\ v_1=0,\ T_1=T_{1w}=T_{1\infty}+b_*x, \\ C_1=C_{1w}=c_*x \quad \text{at} \quad \mathrm{y}=0, \\ u_1\to 0,\ T_1\to T_{1\infty},\ \ C_1\to C_{1\infty}\ \text{ as }\ y\to\infty, \end{aligned} \tag{5}$$

where u_1 and v_1 are the components of dimensional velocities along the x and y directions respectively. T_1 is the fluid temperature, C_1 is the fluid concentration, g is the gravitational acceleration, ν is the kinematic viscosity, β_T is the coefficient of thermal expansion, β_M is the volumetric coefficient of expansion with concentration, B_0 is the constant magnetic field intensity, D_b is the coefficient of mass diffusivity, κ is the thermal conductivity of the fluid, ρ is the density, c_p is the specific heat at constant pressure, V_1^t denotes the thermophoretic velocity and Q_1 is the heat generation.

The radiant heat flux q_h is written as

$$q_h=-\frac{4\sigma_1^*}{3K_1^*}\frac{\partial T_1^4}{\partial y} \tag{6}$$

where σ_1^* is the Stefan-Boltzman constant, K_1^* is the mean absorption coefficient. As stated by Buzuzi *et al.* [4], ${T_1}^4$ can be expressed as a linear combination of the temperatures to give

$$T_1^4\approx -3{T_1}_\infty^4+4{T_1}_\infty^3 T_1 \tag{7}$$

and consequently

$$-\frac{1}{\rho c_p}\frac{\partial q_n}{\partial y}=\frac{16\sigma_1^* {T_1^*}^3_\infty}{3\rho c_p K_1^*}\frac{\partial^2 T_1}{\partial y^2}$$

Hence, equation (3) takes the following form

$$\begin{aligned} u_1\frac{\partial T_1}{\partial x}+v_1\frac{\partial T_1}{\partial y}=\frac{\lambda_c}{\rho c_p}\frac{\partial^2 T_1}{\partial y^2}+\frac{16\sigma_1^* {T_1^*}^3_\infty}{3\rho c_p K_1^*}\frac{\partial^2 T_1}{\partial y^2} \\ +\frac{Q_1(T_1-T_{1\infty})}{\rho C_p}+\frac{\mu}{\rho c_p}\left(\frac{\partial u}{\partial y}\right)^2+\frac{\sigma B_0^2 u_1^2\sin^2\alpha_1}{\rho c_p} \end{aligned} \tag{8}$$

Equations (2) - (4) and boundary conditions (5) are transformed using the following similarity transformations:

$$\begin{aligned} \eta=\left(\frac{a_1}{\nu}\right)^{0.5}f_1,\quad u_1=a_1xf_1',\ v_1=-\left(a_1\nu\right)^{0.5}f_1, \\ T_1-T_{1\infty}=(T_{1w}-T_{1\infty})T(\eta), \\ C_1-C_{1\infty}=(C_{1w}-C_{1\infty})C(\eta), \end{aligned} \tag{9}$$

where $f_1(\eta)$, $T(\eta)$, $C(\eta)$ are the velocity, temperature and concentration distribution fields. Equations (2)- (4)

reduces to the following non-linear, coupled ordinary differential equations:

$$f_1''' + \left(M_pA_1\sin^2\alpha_1 + 1\right)f_1f_1'' - f_1'^2 \quad (10)$$
$$+2A_1f_1f_1'f_1'' - A_1{f_1}^2f_1''' - \left(K_{pp} + M_p\sin^2\alpha_1\right)f_1'$$
$$+\beta_1\left(T\cos\gamma + G_{MT}C\cos\gamma\right) = 0$$

$$T'' + E_{pr}\left[f_1T' + E_c\left(M_p{f_1'}^2 + {f_1''}^2\right) + Q_hT\right] = 0 \quad (11)$$

$$C'' + S_c\left[f_1C' + \tau_1\left(T''C + T'C'\right)\right] - K_mC = 0 \quad (12)$$

such that the following boundary conditions are satisfied:

$$f_1'(\eta) = 1,\ f_1(\eta) = 0,\ T(\eta) = 1,\ C(\eta) = 1 \ \text{ at } \ \eta = 0,$$

$$f_1'(\eta) = 0,\ T(\eta) = 0,\ C(\eta) = 0, \ \text{ as } \ \eta \to \infty, \quad (13)$$

where the prime ($'$) represents differentiation with respect to η and $E_{pr} = P_r/(1 + 4R_p/3)$ denotes the effective Prandtl number, $P_r = \nu\beta_1c_p/\lambda_c$ is the Prandtl number, $R_p = 4\sigma_1^*T_\infty^3\lambda_c/K_1^*$ represents the radiation parameter, $K_{pp} = \nu/K^*a_1$ is the permeability parameter, β_1 represents the local bouyancy number, $M_p = \sigma B_0^2/\rho a_1$ is the Hartman number, $S_c = \nu/D_b$ is the Schmidt number, $A_1 = a_1\lambda_t$ denotes the Deborah number, $Q_h = Q_1/a_1\rho c_p$ represents the heat generation parameter, $G_T = g\beta_T(T_{1w} - T_{1\infty})/\nu^2$ denotes the thermal Grashof number, $G_M = g\beta_M(C_{1w} - C_{1\infty})x^3/\nu^2$ is the solutal Grashof number, $G_{MT} = G_M/G_T = \beta_M(C_{1w} - C_{1\infty})/\beta_T(T_{1w} - T_{1\infty})$ denote the bouyancy ratio, α_1 denotes the magnetic field inclination angle, γ represents the channel inclination angle, $K_m = K_lS_c/a_1$ is the chemical reaction parameter and $\tau_1 = (T_{1w} - T_{1\infty})K_1/T_{1re}$ represents the thermophoretic parameter where K_1 is the thermophoretic coefficient and T_{re} is the reference temperature.

The dimensionless form of the skin friction, heat transfer rate and mass transfer rate are, respectively, $\mathrm{Re}^{1/2}C_f = (1+A_1)\,f_1''(0)$,

$\mathrm{Re}^{-1/2}Nu = -\left(1 + 4R_p/3\right)T'(0)$,

$\mathrm{Re}^{-1/2}Sh = -C'(0)$, where Re is the Reynolds number, C_f is the skin friction coefficient, Nu is the local Nusselt number and Sh is the local Sherwood number.

III. SOLUTION APPROACH

To solve the coupled system of ODE's (10) - (12) we first convert them to first order ODE's as follows. Let $f_1 = y_1,\ f_1' = y_2,\ f_1'' = y_3,\ T = y_4,\ T' = y_5,\ C = y_6$ and $C' = y_7$. The resulting first order ODE's are

$$\frac{df_1}{d\eta} = y_2,$$

$$\frac{d^2f_1}{d\eta^2} = y_3,$$

$$y_3' = \frac{1}{1 - A_1y_1^2}\left[{y_2}^2 + \left(K_{pp} + M_p\sin^2\alpha_1\right)y_2\right]$$
$$-\tfrac{1}{1-A_1f_1^2}\left[\left(M_pA_1\sin^2\alpha_1 + 1\right)y_1y_2 + 2A_1y_1y_2y_3\right]$$
$$-\tfrac{\beta_1}{1-A_1y_1^2}\left[y_4\cos\gamma + G_{MT}C\cos\gamma\right],$$

$$\frac{dT}{d\eta} = y_5$$

$$y_5' = E_{pr}\left[y_1y_5 + E_c\left(M_py_2^2 + y_3^2\right) + Q_hy_4\right]$$

$$\frac{dC}{d\eta} = y_7,$$

$$y_7' = K_my_6 - S_cy_1y_7 + S_c\tau_1\left[y_5y_7 - E_{pr}y_6y_1y_5\right] \quad (14)$$
$$+S_c\tau_1E_cy_6E_{pr}\left[M_py_2^2 + y_3^2\right] + S_cE_{pr}\tau_1Q_hy_6y_4$$

with the following corresponding conditions:

$$y_2(0) - 1,\ y_1(0),\ y_4(0) - 1,\ y_6(0) - 1,$$
$$y_2(10),\ \ y_4(10),\ \ y_6(10). \quad (15)$$

All numerical asymptotic solutions are accurately obtained as long as $\eta_{max} = 10$.

IV. RESULTS AND DISCUSSION

By employing MATLAB software bvp4c the numerical solution to the non-linear ordinary differential equations (10) $-$ (12) are found. Figures 1 $-$ 33 portray the behaviour and impact of the parameters that include the Deborah number A_1, Hartman number M_p, porosity parameter K_{pp}, local bouyancy parameter β_1, bouyancy ratio G_{MT}, chemical reaction parameter K_m, Eckert number E_c, Schmidt number S_c, heat generation parameter Q_h, effective Prandtl number E_{pr}, magnetic field inclination angle α_1, channel inclination angle γ and thermophoretic parameter τ_1 on the velocity, temperature, concentration, skin friction, heat transfer rate and mass transfer rate.

The current calculated numerical values for the heat transfer rate for $R_p = M_p = A_1 = K_{pp} = Q_h = K_m = E_c = 0$ are compared with those reported by Nadeem *et al.* [16] and Wang *et al.* [28] (see Table I) and an excellent agreement is found to exist which validates the accuracy of the numerical method used.

Unless specified, the parameter values used in numerical calculations are $A_1 = 0.2,\ M_p = K_{pp} = K_m = 1,\ \beta_1 = G_{MT} = E_c = S_c = 0.1,\ Q_h = 0.5,\ \tau_1 = 0.2,\ E_{pr} = 0.5,\ \alpha_1 = 90$ and $\gamma = 0$. Figures 1, 11 and 33 illustrates the impact of the Deborah number on the velocity, temperature and concentration of the fluid. It is observed that escalation of the Deborah number results in the decline of the velocity

Table I: Numerical values of the heat transfer rate $-T'(0)$ for $R_p = M_p = A_1 = K_{pp} = Q_h = K_m = E_c = 0$

P_r	Wang [28]	Nadeem *et al.*[16]	Present
0.7	0.4539	0.4582	0.4544
2.0	0.9114	0.9114	0.9114
7.0	1.8954	1.8954	1.8954
20	3.3539	3.3539	3.3539

distribution, rise of the temperature distribution and no effect on the concentration distribution.

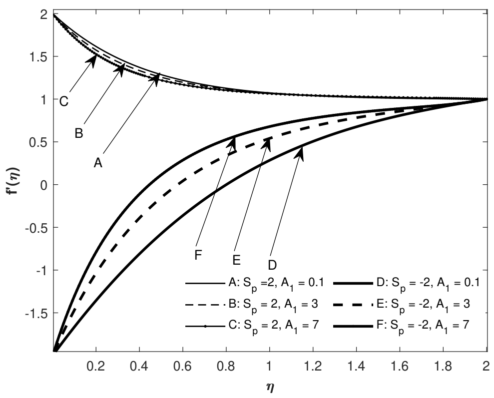

Figure 1: The impact of A_1 on velocity

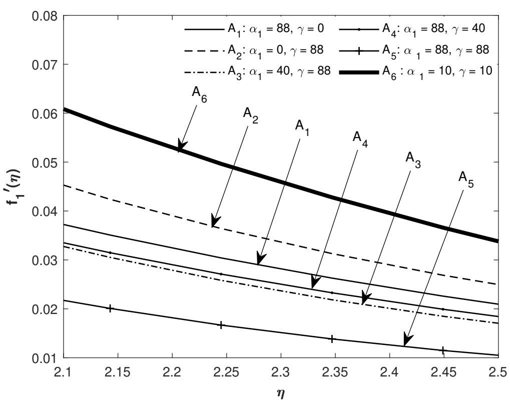

Figure 2: The effect of α_1 and γ on velocity

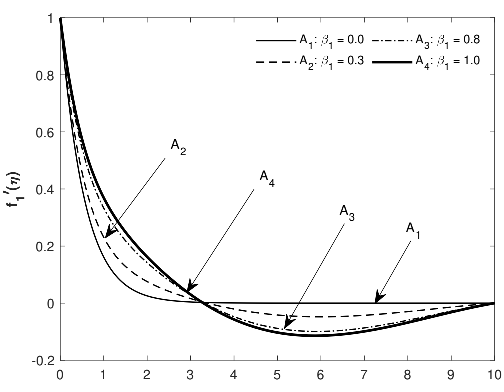

Figure 3: The influence of β_1 on velocity

The role of the magnetic field inclination angle and the channel inclination angle on the velocity, temperature and concentration are depicted in Figures 2, 12, 23, 24, 25 and 26. Figure 2 reveals that the velocity diminishes with increasing values of α_1 and γ. The velocity rises more if $\gamma > \alpha_1$ for any given values of the inclination angles. Temperature profile grows with rising γ values and declines with increasing α_1 values as demonstrated in Figure 12. As is the case with velocity, temperature profiles are bigger whenever $\gamma > \alpha_1$ for any given values of γ and α_1. The temperature distribution is greatest when γ value is maximal and α_1 is minimal, vice versa.

Figures 25 and 26 demonstrates that the concentration is magnified with escalating α_1 and γ values provided $E_{pr} < 1$. However, opposite behaviour is displayed whenever $E_{pr} \geq 1$. Furthermore, Figures 23 and 24 demonstrates that for any α_1 and γ values the concentration profile is larger whenever $\alpha_1 > \gamma$.

The impact of the inclination angles α_1 and γ on the temperature is a function of the E_{pr} value as depicted in Figures 14 and 15. As clearly portrayed in Figure 14 the temperature profile is suppressed for escalating values of α_1 provided $E_{pr} \leq 0.5$, whereas the temperature profile appreciates for enlarged α_1 values provided $E_{pr} > 0.5$. Figure 14 depicts the impact of α_1 on temperature for the case $E_{pr} = 0.5$ and $Epr = 2$. The influence of γ on the temperature of the fluid for varying E_{pr} values is demonstrated in Figure 15. The graphical display reveal that the temperature profile is boosted with increasing γ values for $E_{pr} > 0.6$ and declines for values of $E_{pr} \leq 0.6$. In particular, Figure 15 portrays effect for γ on temperature for the case $E_{pr} = 0.6$ and $E_{pr} = 2$.

The effect of β_1 on the velocity, temperature and concentration is displayed in Figures 3, 13 and 29 respectively. Figure 3 demonstrates that the rise in the value of β_1 enhances the velocity close to the wall with opposite behaviour witnessed further away from the wall. On the contrary, enlargement of β_1 suppresses the temperature closer to the wall with reversed effect further away from the wall. The concentration on the other hand, declines with escalating values of β_1 throughout the boundary layer region as portrayed in Figure 29.

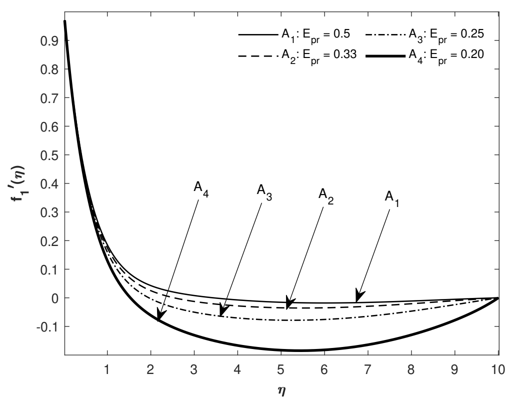

Figure 4: The impact of E_{pr} on velocity

Figures 4, 16 and 30 illustrates the impact of E_{pr} on the velocity, temperature and concentration distribution, respectively. It is observed that increasing values of E_{pr} declines the velocity profile and magnifies the temperature and concentration profiles.

The influence of G_{MT} on the velocity, temperature and concentration distribution is depicted in Figures 5, 17 and 27, respectively. It is clearly revealed that the velocity of fluid is enhanced as G_{MT} value grows. Conversely, the temperature and concentration profiles are suppressed as G_{MT} is enlarged. The temperature exhibit opposite

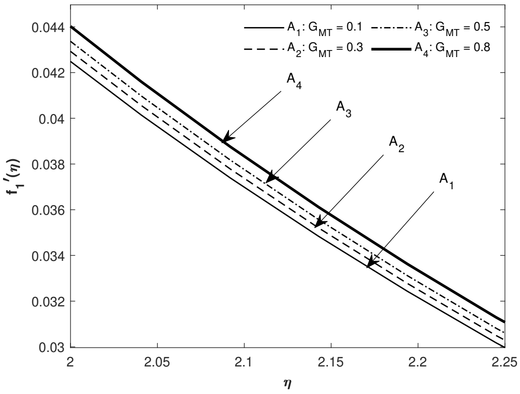

Figure 5: The impact of G_{MT} on velocity

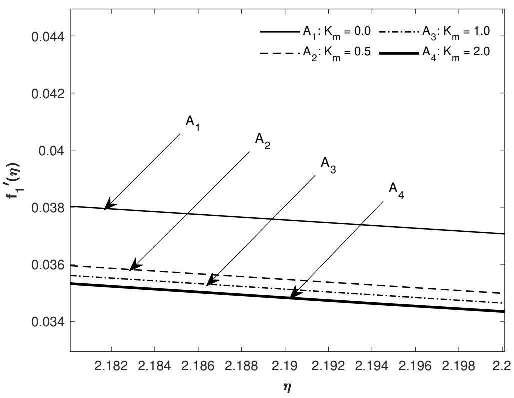

Figure 6: The effect of K_m on velocity

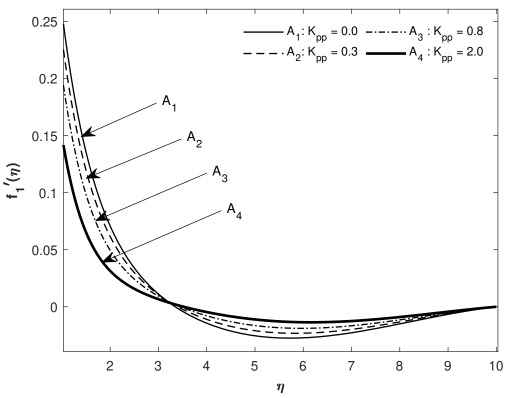

Figure 7: The impact of K_{pp} on velocity

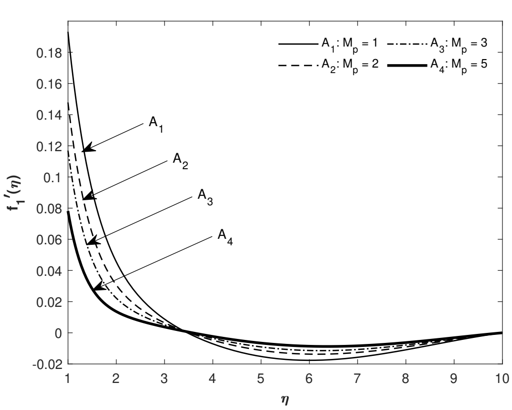

Figure 8: The influence of M_p on velocity

behaviour further away from the wall.

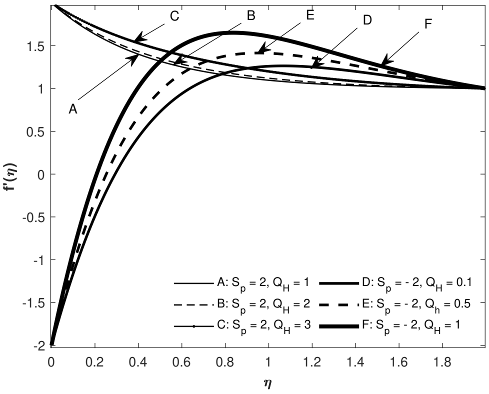

Figure 9: The role of Q_h on velocity

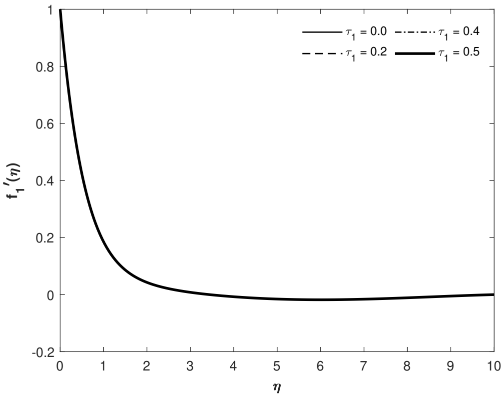

Figure 10: The impact of τ_1 on velocity

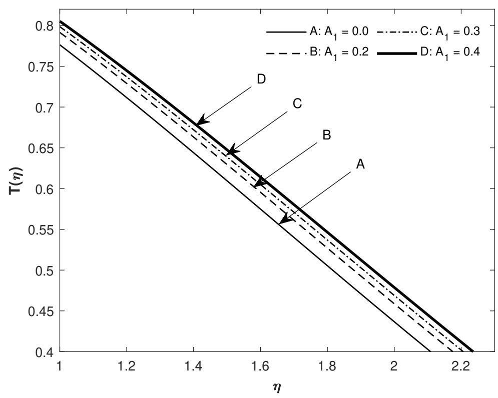

Figure 11: The impact of A_1 on temperature

Figures 6, 18 and 28 are sketched to portray the impact of K_m on the velocity, temperature and concentration profiles respectively. It is noticed that escalating values of K_m suppresses the velocity and concentration distribution. On the other hand, the temperature profile grows with increasing values of K_m.

Figures 7, 19 and 29 demonstrates the influence of K_{pp} on the velocity, temperature and concentration distribution. It is evident that the concentration profile grows with increasing values of K_{pp}. The temperature profiles also grows near the wall ($\eta \leq 5$) and exhibit opposite behaviour further away from the wall. Figure 19 reveals that the the magnitude of the velocity is lowered as K_{pp} increases near the boundary wall ($\eta \leq 2$) and opposite trend is observed at free stream.

The effect of Q_h on the magnitude of the velocity, temperature and concentration of the fluid is exhibited in Figures 9, 21 and 27 respectively. The increasing value of Q_h enhances the velocity and temperature of the fluid. It is also noted that magnifying the value of Q_h grows the concentration profile provided $E_{pr} > 0.5$ with opposite behaviour witnessed when $E_{pr} < 0.5$. The role of M_p on the fluid temperature and concentration is displayed in Figures 8, 20 and 30 respectively. Figure 30 reveals that increasing the magnitude of M_p enhances the fluid concentration. Figures 8 and 20 show that escalating values of M_p magnifies the fluid temperature and diminishes the fluid velocity close to the wall and exhibits opposite behaviour at free stream.

Figures 2, 12, 23, 24, 25 and 26 demonstrates the behaviour of the fluid velocity, fluid temperature and fluid concentration when the inclination angles α_1 and γ are varied at specific E_{pr} values. The fluid velocity is suppressed as α_1 and γ values are enlarged. Figure 2 reveals that the velocity diminishes with increasing values of α_1 and γ. The velocity rises more if $\gamma > \alpha_1$ for any given values of the inclination angles. Temperature profile grows with rising γ values and declines with increasing α_1 values as demonstrated in Figure 12. Similar to the observation on velocity, the temperature profile is bigger whenever $\gamma > \alpha_1$ for any given γ and α_1 values. The temperature distribution is greatest when γ value is maximal and α_1 value is minimal, vice versa. Figures 25 and 26 demonstrates that the fluid concentration is magnified with escalating α_1 values and γ values provided $E_{pr} < 1$. However, opposite behaviour is shown when $E_{pr} \geq 1$. Furthermore, Figures 23 and 24 demonstrates that for any set of α_1 and γ values the fluid concentration profiles are more pronounced whenever $\alpha_1 > \gamma$.

The influence of the thermophoretic parameter τ_1 on the velocity, temperature and concentration profile is depicted in Figures 10, 22 and 32 respectively. It is clear from Figure 10 that varying τ_1 has no effect on the velocity of the fluid. However, enlarged τ_1 values have the effect of retarding the temperature of the fluid as depicted in Figure 22. The concentration of the fluid is raised with escalating values of τ_1 provided $E_{pr} < 1$ and opposite behaviour is witnessed when $E_{pr} > 1$.

The impact of the parameters A_1, α_1, γ, G_{MT}, E_{pr}, Q_h, τ_1, M_p, S_c, E_c, β_1, K_{pp} and K_m on the skin friction $-f_1{}''(0)$, heat transfer $-T'(0)$ and mass transfer rate $-C'(0)$ is portrayed in Tables II, III, IV and V. We infer that, the skin friction is enhanced with the enlargement of the parameters γ, A_1, α_1, K_{pp}, K_m, M_p, S_c and $E_{pr} < 1$. On the contrary, the skin friction declines with the escalation of the parameters Q_h, τ_1, E_c, β_1 and $E_{pr} > 1$.

It is also deduced from the tables that the heat transfer rate is elevated with increase in the parameters $K_{pp} > 1$, E_{pr}, β_1 and τ_1. On the other hand, the magnitude of the heat transfer rate declines with enlarged values of the parameters A_1, α_1, γ, $K_{pp} < 1$, M_p, S_c, E_c and $E_{pr} > 1$. Furthermore, the mass transfer rate rises with growing $E_{pr} > 1$, $K_{pp} < 1$, Q_h, K_m, M_p, S_c, E_c and A_1. The mass transfer rate is suppressed by enlarging γ, $K_{pp} > 1$, E_{pr}, β_1 and τ_1. It is also noted that the impact of G_{MT} on the skin friction, heat transfer rate and mass transfer rate is negligible.

V. CONCLUSIONS

In this study, we have investigated the impact of the channel slope, aligned magnetic field, effective Prandtl number and thermophoresis on MHD Maxwell fluid. The effect of the

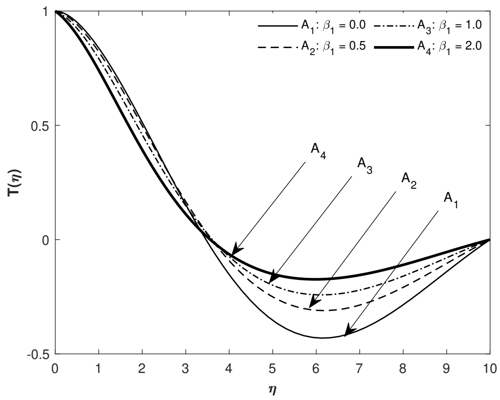

Figure 13: The effect of β_1 on temperature

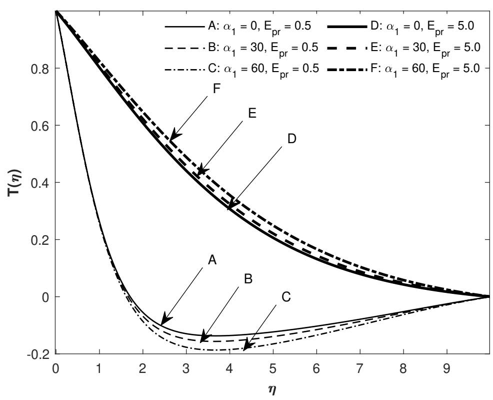

Figure 14: The effect of α_1 on Temperature for varying E_{pr}

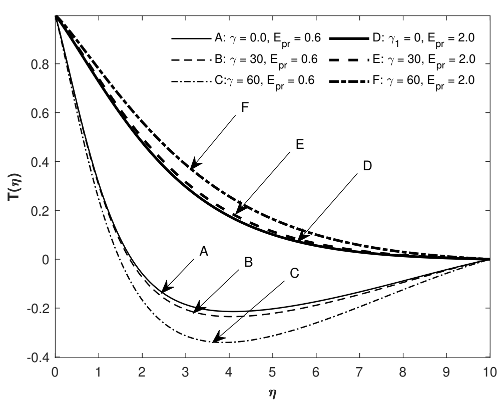

Figure 15: The effect of γ on Temperature for varying E_{pr}

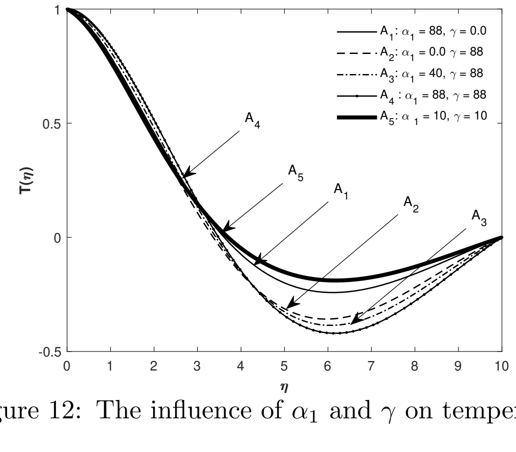

Figure 12: The influence of α_1 and γ on temperature

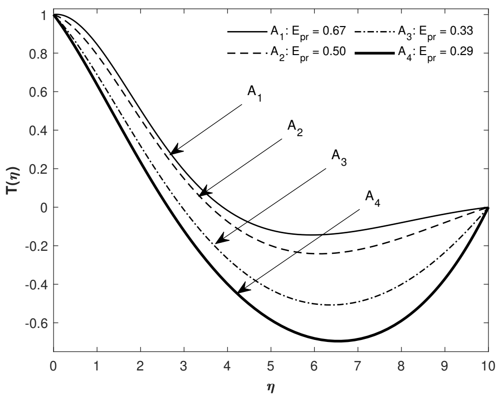

Figure 16: The influence of E_{pr} on the temperature

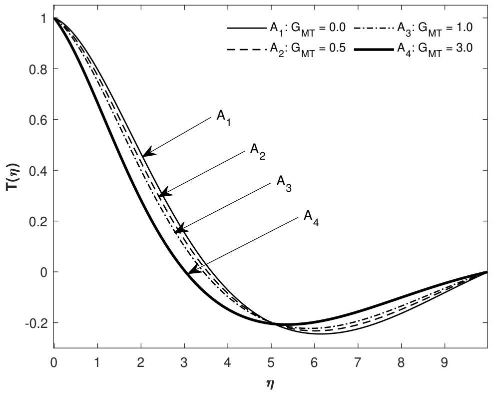

Figure 17:The effect of G_{MT} on temperature

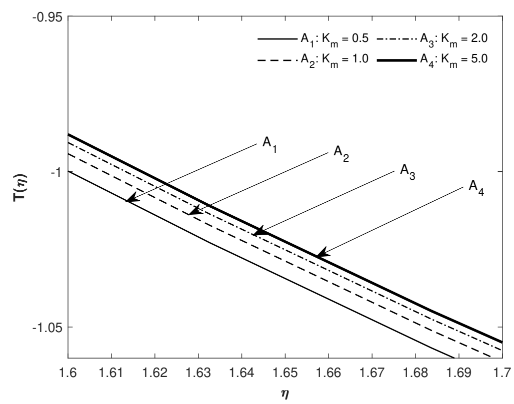

Figure 18:The influence of K_m on temperature

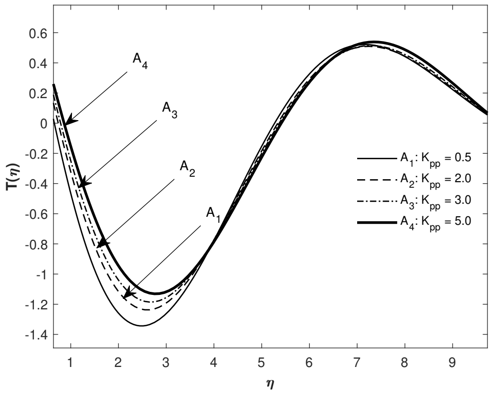

Figure 19: The impact of K_{pp} on temperature

various parameter on the velocity, temperature, concentra-

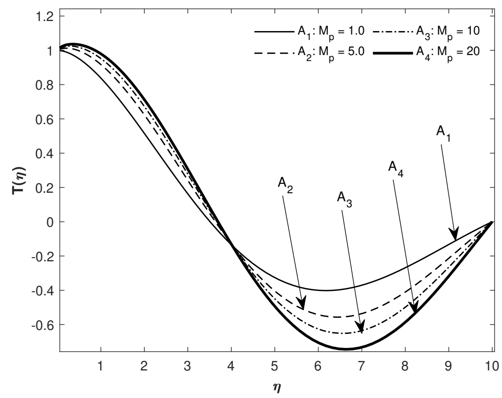

Figure 20: The effect of M_p on temperature

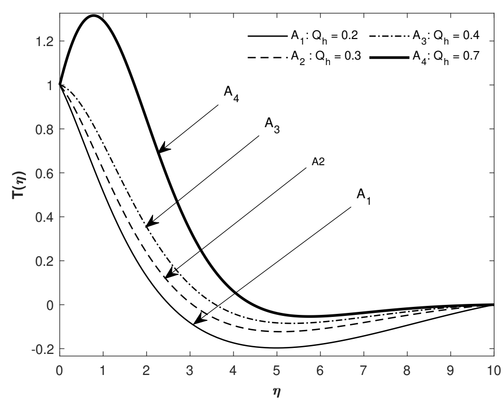

Figure 21:The impact of Q_h on temperature

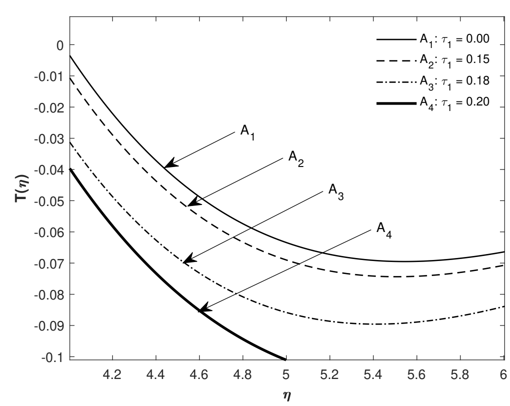

Figure 22: The effect of τ_1 on temperature

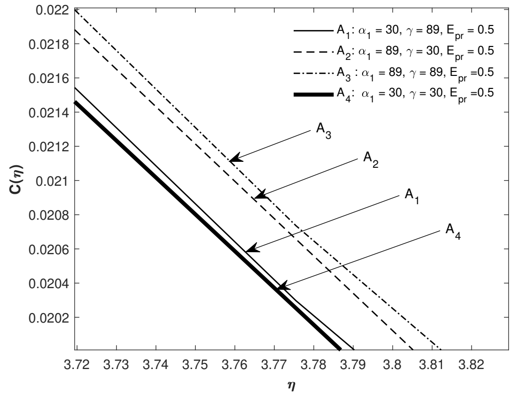

Figure 23: The impact of α_1 and γ on concentration for $E_{pr} = 0.5$

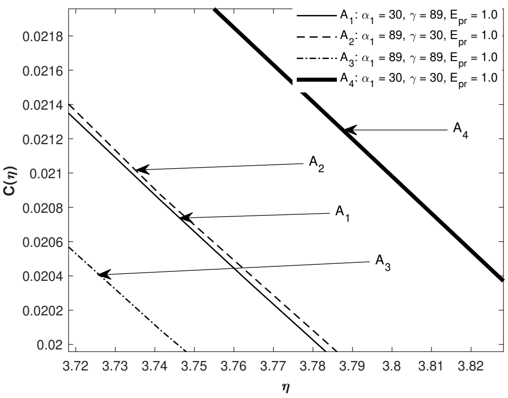

Figure 24: The impact of α_1 and γ on concentration for $E_{pr} = 1$

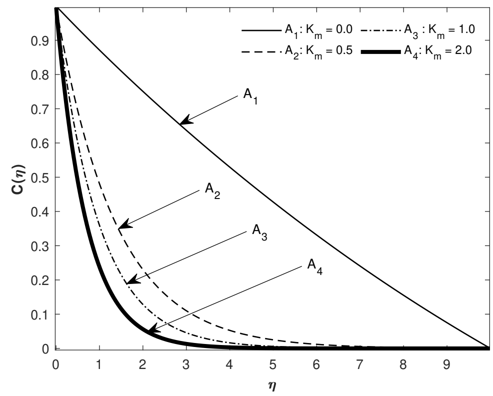

Figure 28: The effect of K_m on concentration

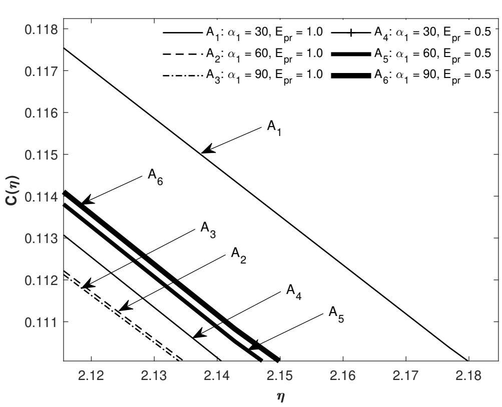

Figure 25: Effect of α_1 on concentration for varying E_{pr}

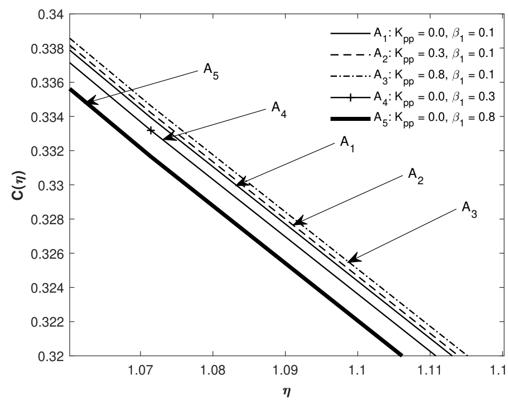

Figure 29: The effect of K_{pp} and β_1 on concentration

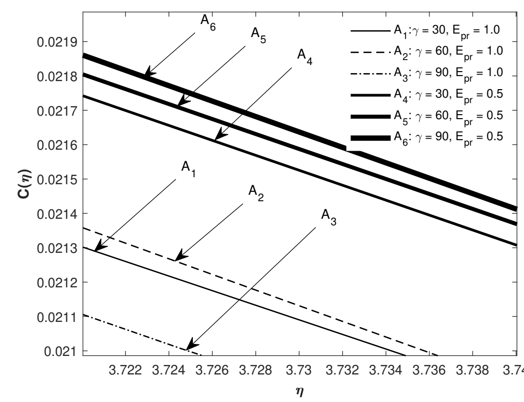

Figure 26: Effect of γ on concentration for varying E_{pr}

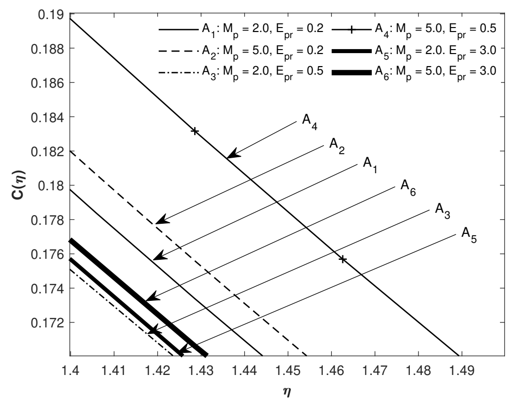

Figure 30: The impact of M_p on Concentration

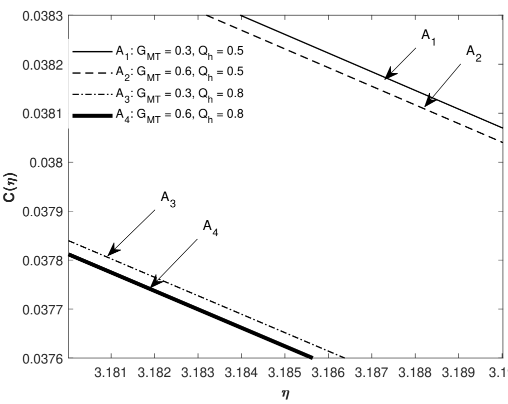

Figure 27: The impact of G_{MT} and Q_h on concentration

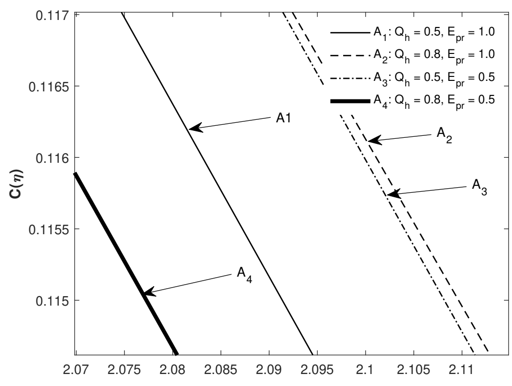

Figure 31: The impact of Q_h with varying E_{pr} on Concentration

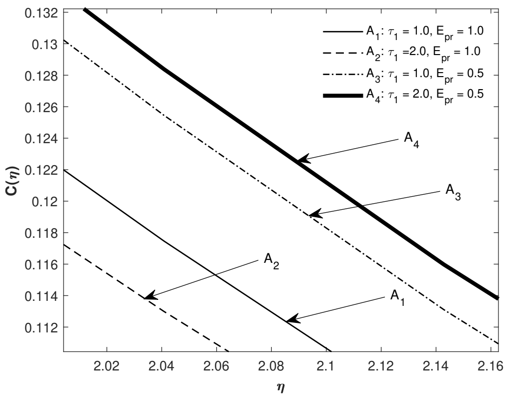

Figure 32: The impact of τ_1 with varying E_{pr} on Concentration

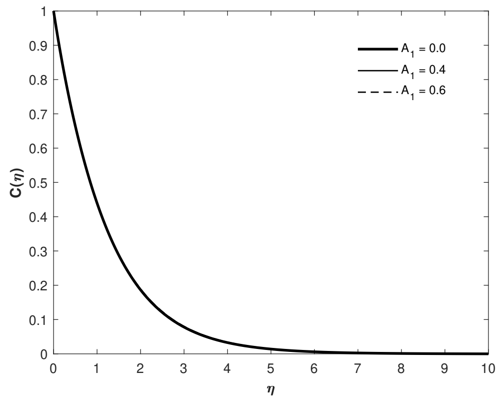

Figure 33: The impact of A_1 on Concentration

Table II: The impact of A_1, α_1, γ and G_{MT} on the skin friction $-f_1{''}(0)$, heat transfer rate $-T'(0)$ and mass transfer rate $-C'(0)$

A_1	α_1	γ	G_{MT}	$-f_1{''}(0)$	$-T'(0)$	$-C'(0)$
0.1	90	30	0.1	1.6722	0.8517	0.7165
0.3				1.7177	0.6564	0.7182
0.5				1.7635	0.5058	0.7195
	60			1.6830	0.6321	0.7185
	30			1.5108	0.8995	0.7165
		60		1.5277	1.2172	0.7132
		90		1.5345	0.0700	0.7250
			0.3	1.5345	0.0700	0.7250
			0.5	1.5345	0.0700	0.7250

tion, skin friction, Nusselt number and Sherwood number are discussed. The main findings of the present analysis are as follows:

1. The magnitude of the fluid velocity is enhanced with rise in the value of $\beta_1,\ A_1,\ Q_h,\ M_p$ for $\eta > 3, K_{pp}$ for $\eta > 3.2$, G_{MT} and E_{pr} and declines with the enlargement of K_m, M_p for $\eta < 3$, K_{pp} for $\eta < 3.2$, γ, α_1, and E_{pr}.
2. The magnitude of the fluid temperature is elevated with increment in the value of the parameters, K_{pp} for $\eta < 5$, M_p for $\eta < 4$, β_1 for $\eta > 3.3$, K_m, A_1, Q_h, E_{pr}, α_1 for $E_{pr} > 0.5$, γ for $E_{pr} > 1$ and G_{MT} for $\eta > 5$ and is lowered with rise in the values of α_1 for $E_{pr} \leq 0.5$, γ for $E_{pr} \leq 1$, K_{pp} for $\eta > 5$, β_1 for $\eta \leq 3.3$, G_{MT} for $\eta \leq 5$ and M_p for $\eta > 4$.
3. The fluid concentration rises with escalation of the parameters $K_{pp},\ M_p,\ E_{pr},\ Q_h$ for $E_{pr} > 0.5$, α_1 for $E_{pr} < 1$, γ for $E_{pr} < 1$ and τ_1 for $E_{pr} \leq 5$ and diminishes with the growing values of $\beta_1,\ G_{MT},\ K_m,\ Q_h$ for $E_{pr} \leq 0.5$, α_1 for $E_{pr} \geq 1$, γ for $E_{pr} \geq 1$ and τ_1 for $E_{pr} > 0.5$.

Table III: The impact of E_{pr}, Q_h, τ_1 and K_m on the skin friction $-f_1{''}(0)$, heat transfer rate $-T'(0)$ and mass transfer rate $-C'(0)$

E_{pr}	Q_h	τ_1	K_m	$-f_1{''}(0)$	$-T'(0)$	$-C'(0)$
2.0	0.2	0.15	0.5	1.6722	0.8517	0.7165
1.0				1.6642	0.5830	0.7192
0.5				1.6880	1.1805	0.7133
	0.3			1.6631	0.5352	0.7196
	0.4			0.6529	0.2380	0.7226
	0.5			1.6463	0.0238	0.7248
		0.18		1.6529	0.2380	0.7223
		1.0		1.6529	0.2381	0.7167
				1.5345	0.0700	0.7250
			1.0	1.6529	0.2376	1.0029
			1.5	1.6536	0.2374	1.2256
			2.0	1.6538	0.2373	1.4136

Table IV: The impact of M_p, S_c, E_c and β_1 on the skin friction $-f_1{''}(0)$, heat transfer rate $-T'(0)$ and mass transfer rate $-C'(0)$

M_p	S_c	E_c	β_1	$-f_1{''}(0)$	$-T'(0)$	$-C'(0)$
1	0.1	0.1	0.1	1.6722	0.8517	0.7165
3				2.1887	0.0561	0.7230
5				2.6142	-0.3050	0.7257
	0.3			2.6142	-0.3052	0.7632
	0.5			2.6142	-0.3054	0.8011
		0.3		2.6107	-1.2057	0.8629
		0.5		2.6072	-2.1028	0.9245
			0.2	2.5666	-2.0107	0.9208
			0.3	2.5273	-1.9369	0.9180

Table V: The impact of K_{pp} on the skin friction $-f_1{''}(0)$, heat transfer rate $-T'(0)$ and mass transfer rate $-C'(0)$

K_{pp}	$-f_1{''}(0)$	$-T'(0)$	$-C'(0)$
0.8	1.5345	0.0700	0.7250
0.9	1.5665	0.0186	0.7254
1.0	1.5980	0.0457	0.7259
2.0	1.8842	0.6028	0.7181

4. The optimal value of the fluid velocity is attained when both α_1 and γ are maximal. On the other hand, the fluid temperature is greatest when γ is maximum and α_1 is minimal. The fluid concentration is highest when either both α_1 and γ are minimal provided $E_{pr} \geq 1$ or when both α_1 and γ are maximal provided $E_{pr} < 1$. For any combination of of α_1 and γ values the velocity and temperature profiles are bigger whenever $\gamma > \alpha_1$. On the contrary, the concentration profile is bigger whenever $\alpha_1 > \gamma$.
5. Escalating the value of the parameters $\gamma,\ A_1,\ \alpha_1,\ K_{pp},\ K_m,\ M_p,\ S_c$ and $E_{pr} < 1$ have the effect of enhancing the skin friction. On the other hand, the skin friction diminishes with increasing value of $Q_h,\ \tau_1,\ E_c,\ \beta_1$ and $E_pr > 1$.
6. The heat transfer rate is elevated with enlarged values

of $K_{pp} > 1$, E_{pr}, β_1 and τ_1 and is reduced with rising value of A_1, α_1, γ, $K_{pp} < 1$, M_p, S_c, E_c and $E_{pr} > 1$.

7. The mass transfer rate grows with increasing values of $E_{pr} > 1$, $K_{pp} < 1$, Q_h, K_m, M_p, S_c, E_c and A_1 and is reduced with increasing value of γ, $K_{pp} > 1$, E_{pr}, β_1 and τ_1. There is considerable agreement between our present investigation and findings in previously published literature. Outstanding findings in this study are that for enlarged values of Q_h the fluid concentration is enhanced provided $E_{pr} > 0.5$. The fluid concentration also rises with increasing values of γ and α_1 whenever $E_{pr} < 1$. On the other hand, the magnitude of the fluid temperature is greatest when γ is maximal and α_1 is minimal. The temperature profile is boosted when the values of α_1 and γ are raised for higher E_{pr} values ($E_{pr} > 0.5$ for α_1 and $E_{pr} > 1$ for γ) and the temperature depreciates for lesser E_{pr} values. Furthermore, it is noticed that for any given set of γ and α_1 values the magnitude of the fluid velocity and the fluid temperature is greater whenever $\gamma > \alpha_1$. Also for any combination of the inclination angles α_1 and γ the fluid concentration is greater whenever $\alpha_1 > \gamma$. The effect of τ_1 on the temperature and concentration profile is a function of the E_{pr} value and it depends on whether the E_{pr} value is greater or less than unity.

REFERENCES

[1] M. S. Alam, M. M. Rahman, and A. Satter, “Transient magnetohydrodynamic free convective heat and mass transfer flow with thermophoresis past a radiate inclined permeable plate in the presence of variable chemical reaction and temperature dependent viscosity”, Nonlinear Analysis: Model Control, vol. 14, pp. 3-20, 2009.

[2] Y. Boi, Y. Jiang, F. Liu, and Y. Zhang, ”Numerical analysis of fractional MHD Maxwell fluid with the effects of convection heat transfer condition and viscous dissipation,” AIP Advances, vol7, 125309, 2017.

[3] G. Buzuzi and A. N. Buzuzi, “Unsteady MHD convection flow and heat transfer past a vertical inclined plate in a porous medium with variable plate temperature with suction in a slip flow regime”, Int. J. of Appl. Math., vol. 32, no. 2, pp. 205-218; DOI: 10.12732/ijam.v32i2.4, 2019.

[4] G. Buzuzi, G. Makanda, “Numerical analysis on unsteady MHD flow and heat transfer over an inclined stretching surface in a porous medium with heat source and variable magnetic field angle”, International Journal of Applied Mathematics, vol. 35, no. 2, pp. 205-223, 2022.

[5] G. Buzuzi, “Inclined magnetic field and effective Prandtl number effects on unsteady MHD oscillatory flow past an inclined surface with constant suction and chemical reaction”, Journal of the Nigerian mathematical Society, vol. 40, no. 3, 227-244, 2021.

[6] G. Buzuzi, ”Unsteady MHD Casson Fluid Flow Past an Inclined Surface Subjected to Variable Magnetic Field, Heat Generation and Effective Prandtl Number,” Engineering Letters, vol. 31, no.2, pp. 627-639, 2023.

[7] A. Dadheech, A. Parmar, A. Olkha, ” Inclined MHD and radiative Maxwell slip fluid flow and heat transfer due to permeable melting surface with a non-linear heat source,” International Journal of Applied and Computational Mathematics, vol. 7, Article number 89, 2021

[8] U. Farooq, D. Lu , S. Munir, M. Ramzan, M. Suleman, and S. Hussain, ”MHD flow of Maxwell fluid with nanomaterials due to an exponentially stretching surface” Scientific Reports, vol. 9:7312, https://doi.org/10.1038/s41598-019-43549-0, 2019.

[9] C. Fetecau, R. Ellahi, and S. M. Sait, ”Mathematical analysis of Maxwell fluid flow through a porous plate channel induced by a constantly accelerating oscillating wall,” Mathematics, vol. 9, no. 1, pp. 90, 2021.

[10] A. Haritha, Y. Devasena, and B. Vishali, ”MHD heat and mass transfer of the unsteady flow of a Maxwell fluid over a stretching surface with Navier slip and convective boundary conditions,” Global Journal of Pure and Applied mathematics, vol. 13, pp. 2169-2179, 2017.

[11] K. Loganathan, N. Alessa, N. Namgyel, and T. S. Karthik, ”MHD flow of thermally radiative Maxwell fluid past a heated stretching sheet with Catteneo-Christov dual diffusion,” Handawi Journal of Mathematics, vol. 2021, https://doi.org/10.1155/2021/5562667, 2021.

[12] K. Loganathan, K. Mohana, M. Mohanraj, P. Sakthivel, and S. Rajan, ”Impact of third-grade nanofluid flow across a convective surface in the presence of inclined Lorentz force: an approach to entropy optimization,” Journal of Thermal Analysis and Calorimetry, vol. 144, no. 5, pp. 1935-1947, 2020.

[13] K. Loganathan, S. Sivasankaran, M. Bhuvaneswari, and S. Rajan, ”Secod-order slip, cross-diffusion and chemical reaction effects on magneto-convection of Oldroyd-B liquid using Cattaneo-Christov heat flux with convective heating,” Journal of Thermal Analysis and Calorimetry, vol. 136, no. 1, pp. 401-409, 2019.

[14] E. Mgyari, “Comment on ” Mixed convection boundary layer flow over a horizontal plate with thermal radiation by A Ishak, Heat mass Transfer, DOI 10.1007/s00231-009-0552-3”, Heat Mass Transfer, vol. 46, pp. 509-810, 2010.

[15] E. Magyari, and A. Pantokratoras, “Note on the effect of thermal radiation in the linearized Roseland approximation on the heat transfer characteristics of various boundary layer flows”, International Communications in Heat and Mass Transfer, vol. 38, pp. 554-556, 2011.

[16] S. Nadeem, R. U. Haq, and C. Lee, “Numerical study of MHD boundary layer flow of a Maxwell fluid past a stretching sheet in the presence of nanoparticles ”, Journal of the Taiwan Institute of Chemical Engineer, vol. 45, pp. 121-126, 2013.

[17] N. F. M. Noor, ” Analysis for MHD flow of a Maxwell fluid past a vertical stretching sheet in the presence of thermophoresis and chemical reaction”, World Academy of Science, Engineering and Technology, vol. 64, pp. 1019-1023, 2012.

[18] H. Qi and M. Xu, ”Unsteady flow of viscoelastic fluid with fractional Maxwell model in a channel,” Mechanics Research Comminications, vol. 34, no. 2, pp. 210-212, 2007.

[19] C. S. K. Raju, N. Sandeep, C. Sulochana, V. Suganamma and M. Jayachandra, “Radiation, inclined magnetic field and cross-diffusion effects on flow over a stretching surface”, Journal of the Nigerian Mathematical Society, vol. 34, pp. 169-180, 2015.

[20] M. Ramzan, A. Shafique, M. Rasid, M. Nazar, Z. U. Nisa, ”Slippage flow of Maxwell fluid over an inclined vertical plate with generalized heat and mass transfer,”

Journal of Advanced Research in Fluids Mechanics and Thermal Sciences, vol. 99, no. 2, pp. 155-167, 2022.

[21] S. Saleem, M. Awaias, S. Nadeem, N. Sandeep, and M. T. Mustafa, " Theoretical analysis of upper-converted Maxwell fluid flow with Cattaneo-Christov heat flux model," Chinese Journal of Physics, vol. 55, no. 4, pp. 1615-1625, 2017.

[22] N. Sandeep and V. Sugunamma, "Radiation and inclined magnetic field effects on unsteady hydromagnetic free convection flow past an impulsively moving vertical plate in a porous medium", J. Appl. Fluid. Mech, vol. 7, no. 2, pp. 275-286, 2014.

[23] N. Sandeep and C. Sulochana, "Momentum and heat transfer behaviour of Jeffrey, Maxwell and Oldroyd-B nanpfluids past a stretching surface with non-uniformheat source/sink," Ain Shams Engineering Journal, vol. 9, no. 4, pp. 517-524, 2018.

[24] S. Sharidan, T. Mahmood, I. Pop, "Similarity solutions for the unsteady boundary layer flow and heat transfer due to a stretching sheet", International Journal of Mechanics and Engineering, vol. 11, no. 3, pp. 647-654, 2006.

[25] C. Sivaraj, and M. A. Sheremet, "MHD natural convection in an inclined square porous cavity with a heat conducting solid block", Journal of Magnetism and Magnetic materials, vol. 426, pp. 351-360, 2017.

[26] X. Sun, S. Wang, and M. Zhao, "Oscillatory flow of Maxwell fluid in a tube of isosceles right triangles cross section," Physics of Fluids, vol. 31, Article ID 123101, 2019.

[27] M. J. Uddin, "Convective flow of micropolar fluids along an inclined flat plate with variable electric conductivity and uniform surface heat flux", DAFFODIL Int. Univ. J. of Sci. and Techn., Vol. 6, no. 1, pp. 69-79, 2011.

[28] C. G. Wang, "Free convection on a vertical stretching surface", J Appl Math Mech., vol. 69, pp. 418-420, 1989.

[29] S. Wang, P. Li, M. Zhao, "Analytical study of oscillatory flow of Maxwell fluid through a rectangular tube," Physics of Fluids, vol. 31, Article ID 063102, 2019.

[30] T. Wenchaang, P. Wenxiao, and X. Mingyu, "A note on unsteady flows of a viscoelastic fluid with the fractional Maxwell model between two parallel plates," International Journal of Non-linear Mechanics, vol. 38, no. 5, pp. 645-650, 2003.